Narrow-Waisted Gaussian Beam Discretization for Short-Pulse Radiation From One-Dimensional Large Apertures

Vincenzo Galdi, *Member, IEEE*, Leopold B. Felsen, *Life Fellow, IEEE*, and David A. Castañon, *Senior Member, IEEE*

***Abstract*—In this paper, we develop a Gabor-based Gaussian Beam (GB) algorithm for representing two-dimensional (2-D) radiation from finite aperture distributions with short-pulse excitation in the time domain (TD). The work extends previous results using 2-D frequency-domain (FD) narrow-waisted Gaussian beams [1]. The FD algorithm evolves from the rigorous Kirchhoff integration over the aperture distribution, which is then parameterized via the discrete Gabor basis and evaluated asymptotically for high frequencies to furnish the GB propagators to the observer. The TD results are obtained by Fourier inversion from the FD and yield pulsed beams (PB). We describe the resulting TD algorithm for several aperture distributions, ranging from simple linearly phased (linear delay) to arbitrary time delay profiles; the latter accommodate the important case of focusing TD aperture fields. For modulated pulses with Gaussian envelopes, we compute accurate closed form analytic solutions, which have been calibrated against numerical reference data. Our results confirm that the previously established utility of the Gabor-based narrow-waisted FD-GB algorithm for radiation from distributed apertures [1] remains intact in the TD.**

***Index Terms*—Gabor lattice representations, Gaussian beams (GBs), pulsed beam wavepackets.**

I. Introduction

GAUSSIAN beams (GBs) have been used *conventionally* as *highly collimated* basis elements in a variety of frequency domain (FD) and time domain (TD) radiation, propagation and scattering scenarios, especially in the asymptotic high frequency (HF) regime. The bases can be continuous or discrete, the latter being anchored to a Gabor lattice in the (physical-domain)–(spectral domain) FD or TD phase space [2]–[10]. When applied to radiation from extended GB-parameterized aperture distributions, the radiated fields at the observer are synthesized by summation over the individual basis beam contributions. When interacting with a complex propagation or scattering environment, the (localization) resolution capabilities of the GB algorithms are essentially on the order of the collimation width of the basis beams, which generally extends over many wavelengths. This is in contrast to HF ray-based algorithms that explore local properties of the environment, but have deficiencies due to failures in ray-optical transition regions near shadow boundaries, caustics, etc. A *nonconventional* form of the Gabor algorithm, which uses *narrow-waisted poorly collimated* basis beams, simulates ray-like behavior without the transition region failures of ray fields. In the FD, the collective effect of the narrow-waisted nonconventional Gabor-stacked basis beams has been shown capable of furnishing highly accurate and numerically efficient solutions for scattering by, or transmission through, complex environments irradiated by aperture distributions [11]–[14]; this renders the algorithm useful as an efficient forward solver for inverse scattering and reconstruction [15].

In this paper, we extend the FD Gabor-based narrow-waisted beam algorithm for radiation from extended apertures [1] to the TD. The initial Kirchhoff integration over the FD aperture distribution is parameterized via the discrete Gabor basis and reduced by high frequency asymptotics to furnish the GB propagators to the observer; the TD pulsed beam (PB) propagators are obtained by Fourier inversion from the FD. For insight into the analytic implications and physical interpretation of the FD-inverted integrals, various aperture distributions are analyzed, starting from linearly phased (linear delay) to arbitrary time delay profiles; the latter are illustrated by the important example of focusing TD aperture fields. Accurate and easily computable closed-form analytic solutions are obtained for modulated pulses with Gaussian envelopes and are calibrated against independently generated numerical reference data. These results confirm that the previously established utility of the Gabor-based narrow-waisted FD–GB algorithm for radiation from distributed apertures [1] remains intact in the time domain.

In the FD, it has been established that the GB basis beams can be tracked efficiently from the aperture through interactions with complex scattering environments [11]–[14] and are therefore useful forward solvers in inversion scenarios [15]. Interaction of the PB propagators with complex environments is presently under consideration.

The rest of this paper is organized as follows. Section II has a compact summary of the FD formulation and its asymptotic re-

Manuscript received September 19, 2000; revised February 28, 2001. This work was supported by ODDR&E under MURI Grants ARO DAAG55-97-1-0013, by AFOSR F49620-96-1-0028, and by the Engineering Research Centers Program of the National Science Foundation under award number EEC-9986821. The work of V. Galdi was supported by a European Union postdoctoral fellowship through the University of Sannio, Benevento, Italy. The work of L. B. Felsen was supported in part under Grant 9900448 by the US-Israel Binational Science Foundation, Jerusalem, Israel, and from Polytechnic University, Brooklyn, NY, USA.

V. Galdi is with the Department of Electrical and Computer Engineering, Boston University, Boston, MA 02215 USA and with the University of Sannio, Benevento, Italy (e-mail: vgaldi@bu.edu).

L. B. Felsen is with the Department of Aerospace and Mechanical Engineering and the Department of Electrical and Computer Engineering, Boston University, Boston, MA 02215 USA and Polytechnic University, Brooklyn, NY 11201 USA (e-mail: lfelsen@bu.edu).

D. A. Castañon is with the Department of Electrical and Computer Engineering, Boston University, Boston, MA 02215 USA (e-mail: dac@bu.edu).

Publisher Item Identifier S 0018-926X(01)07643-8.

duction for narrow-waisted basis beams; the results are applied to linearly phased apertures (which includes the nonphased special case). Section III is concerned with the inversion to the TD, treating in sequence space–time separable linear-delay and nonlinear-delay aperture field profiles. The analytic reduction of the GB inversion integrals for modulated Gaussian envelope pulsed beams (PB) is presented succinctly, with details relegated to several appendixes. Simplifying approximations are stated. The resulting constraints on the range of validity of the algorithms are assessed analytically and phrased concisely in terms of critical nondimensional estimators. Calibration/confirmation is implemented through a sequence of numerical tests and examples, including radiation from a cosine-tapered aperture distribution with nonlinear (quadratic) delay, which is tracked as the wavefield approaches, reaches, and propagates beyond, the focal plane. Snapshots in the examples are resolved in terms of spatial and temporal cuts that depict the spatial and temporal deformations along the propagation path of the pulsed wavefield. Conclusions are presented in Section IV.

II. Frequency Domain Formulation

We briefly summarize the frequency domain (FD) formulation, and refer the interested reader to [1]–[4], [11], [12] for details. We restrict ourselves to the 2-D (x, z) domain, with all configurational quantities independent on y. Excitation is specified as a y-directed electric field with implicit time-harmonic dependence $\exp(-i\omega t)$ and spatial distribution $F(x, \omega)$, which occupies the aperture region $|x| \leq d/2$ at $z = 0$

$$E_y(x, z = 0, \omega) = F(x, \omega), \qquad |x| \leq d/2. \tag{1}$$

The aperture geometry is shown in Fig. 1. The resulting (TM polarized) electromagnetic (EM) field radiated into the half-space $z > 0$ can be expressed by line-source superposition (Kirchhoff integration) in physical space

$$E_y(x, z, \omega) = -2\frac{\partial}{\partial z}\int_{-d/2}^{d/2} F(x', \omega) G_{2\mathrm{D}}(kR)\, dx'$$

$$G_{2\mathrm{D}}(kR) = \frac{i}{4}\mathrm{H}_0^{(1)}(kR) \tag{2}$$

$$\mathbf{H} = \frac{1}{i\omega\mu_0}\nabla \times E_y \mathbf{u}_y = H_x \mathbf{u}_x + H_z \mathbf{u}_z \tag{3}$$

where

$k = \omega\sqrt{\epsilon_0\mu_0} = 2\pi/\lambda$	free-space wavenumber, with λ as the wavelength;
$\mathbf{u}$	denotes a unit vector;
$\mathrm{H}_0^{(1)}(\cdot)$	zeroth order Hankel function of the first kind;

and (in accord with the radiation condition)

$$R = \sqrt{(x - x')^2 + z^2} \geq 0. \tag{4}$$

In the remainder of this section, the ω dependence in E_y and F will be omitted in the notation. Equation (2) is derived using the free-space 2-D Green's function $G_{2\mathrm{D}}(R)|_{z'=0}$ to simulate an equivalent magnetic line dipole current distribution on an electric wall boundary.

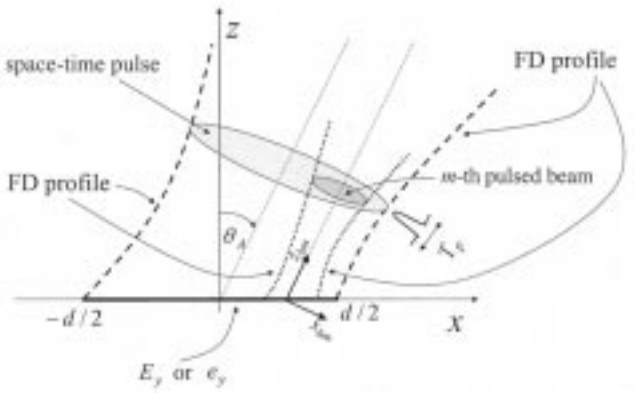

Fig. 1. Aperture geometry, global coordinates and beam coordinates for a tapered linearly phased aperture field distribution. FD: $F(x, \omega) = P(\omega)g(x)\exp(ikx\sin\theta_A)$ [see (29)]. TD: $f(x, t) = g(x)p(t - c^{-1}x\sin\theta_A)$ [see (28)].

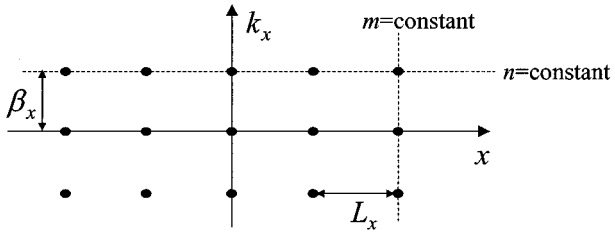

Fig. 2. Discretized Gabor lattice in the (x, k_x) phase space, where k_x is the x-domain wavenumber. $n = \mathrm{const.}$: spatially displaced beams centered at $x_m = mL_x$, with fixed phase gradient (beam tilt) $(n\beta_x)$; $m = \mathrm{const.}$: spectrally displaced beams with beam tilts $(n\beta_x)$ at fixed location x_m.

A. FD Beam Discretization

1) Aperture Field: The aperture field $F(x)$ is to be parameterized in terms of GB basis functions via the rigorous self-consistent Gabor series representation [16], [17]

$$F(x) = \sum_{m,n=-\infty}^{\infty} A_{mn} w(x - mL_x)\exp(in\beta_x x) \tag{5}$$

where $w(x)$ represents the normalized Gaussian window (initial beam profile)

$$w(x) = \left(\frac{\sqrt{2}}{L_x}\right)^{1/2}\exp\left[-\pi(x/L_x)^2\right]$$

$$\int_{-\infty}^{\infty} w^2(x)\, dx = 1. \tag{6}$$

This representation places the beam basis functions on a discretized (x, k_x) phase-space lattice (see Fig. 2), on which each lattice point gives rise to a GB, whose spatial and spectral (beam tilt) shifts are tagged by the indexes m and n, respectively. Spatial and spectral periods are related by the self-consistency relation (configuration-spectrum tradeoff) $L_x\beta_x = 2\pi$ [16], [17]. The expansion coefficients in (5) can be computed by introducing an auxiliary *bi-orthogonal* function $\gamma(x)$ [16], [17]

$$A_{mn} = \int_{-\infty}^{\infty} F(x)\gamma^*(x - mL_x)\exp(-in\beta_x x)\, dx \tag{7}$$

but as shown below, our subsequent use of narrow-waisted beams avoids the cumbersome computation of γ and numerical implementation of (7). Combining (2) and (5) yields the Gabor lattice representation of the aperture field.

2) Radiated Field: The corresponding Gabor lattice representation for the field radiated into the half-space $z > 0$ is given by [1]

$$E_y(x, z) = \sum_{m,\, n=-\infty}^{\infty} A_{mn} B_{mn}(x, z) \tag{8}$$

where the beam functions $B_{mn}(x, z)$ are expressed by Gabor-weighted line-source superposition

$$B_{mn}(x, z) = -\frac{i}{2} \int_{-d/2}^{d/2} w(x' - mL_x) \times \exp(in\beta_x x') \frac{\partial}{\partial z} \mathrm{H}_0^{(1)}(kR)\, dx' \tag{9}$$

R being defined in (4). By saddle point methods, the integral in (9) (or its spectral counterpart) can be evaluated asymptotically in the beam *paraxial far zone*, yielding the following *complex source point* (CSP) approximation [11], [12]

$$B_{mn}(x, z) \sim -ik2^{5/4} \left(\frac{L_x}{8\pi k}\right)^{1/2} \times \exp\left\{i\left[k\left(\tilde{R}_{mn} + ib_n\right) + \pi/4\right]\right\} \frac{(z - \tilde{z}'_{mn})}{\tilde{R}_{mn}^{3/2}} \tag{10}$$

with $\tilde{R}_{mn}$ representing the *complex distance*

$$\tilde{R}_{mn} = \overline{P_o \tilde{P}'_{mn}} = \sqrt{(x - \tilde{x}'_{mn})^2 + (z - \tilde{z}'_{mn})^2} \tag{11}$$

between the observer at $P_o = (x, z)$ and the *complex source point* (CSP), $\tilde{P}'_{mn} = (\tilde{x}'_{mn}, \tilde{z}'_{mn}) = (mL_x + ib_n \sin\theta_n, ib_n \cos\theta_n)$, where, in accord with the radiation condition [see (4)], the square root is defined by $\mathrm{Re}(\tilde{R}_{mn}) \geq 0$. Here and henceforth, the tilde $\sim$ denotes a complex quantity. The CSP displacement parameter (Fresnel length) b_n is related to the beam lattice period L_x and the beam axis angle $\theta_n = \sin^{-1}(n\lambda/L_x)$ via $b_n = (L_x \cos\theta_n)^2/\lambda$ [11], and (10) is valid in the paraxial far-zone of each beam, $|\tilde{R}_{mn}| \gg b_n$. As the tilt index n increases to $|n| > L_x/\lambda$, the beam tilt angle θ_n becomes complex, and the corresponding beams become *evanescent*.

B. Narrow-Waisted Beams

As emphasized in [1], [11], and [12], *narrow-waisted* beams ($L_x \lesssim \lambda \ll d$) have several attractive features. First, the Gabor coefficients can be estimated with good approximation by *sampling* the aperture field distribution, avoiding the time-consuming integration (7) [1]

$$A_{mn} \approx \begin{cases} \left(L_x/\sqrt{2}\right)^{1/2} F(mL_x), & n = 0 \\ 0, & n \neq 0 \end{cases} \tag{12}$$

so that

$$E_y(x, z) \approx \sum_{|m| \leq (d/2L_x)} A_{m0} B_{m0}(x, z) \tag{13}$$

$$B_{m0}(x, z) \sim -ik2^{5/4} \left(\frac{L_x}{8\pi k}\right)^{1/2} \times \exp\left\{i\left[k\left(\tilde{R}_{m0} + ib\right) + \pi/4\right]\right\} \frac{(z - ib)}{\tilde{R}_{m0}^{3/2}} \tag{14}$$

$$\tilde{R}_{m0} = \sqrt{(x - mL_x)^2 + (z - ib)^2} \tag{15}$$

$$b = b_0 = L_x^2/\lambda. \tag{16}$$

In this approximation, the tilted ($n \neq 0$) beams in the Gabor expansion, which generate evanescent "far fields" for $L_x/\lambda < |n|$, are ignored. Second, for narrow-waisted beams, the CSP paraxial *far-zone* approximation (10) can be invoked at *moderate* distance and, therefore, the paraxial beam superposition gives accurate results even in the *near zone* of the *aperture*. Third, as shown in [11]–[14], interaction of narrow-waisted beams with an environment can be effectively tracked by *complex ray asymptotics*.

C. Linearly Phased Aperture

As shown in [1] and [11], narrow-waisted beams work very well for nonphased apertures, but usually require finer aperture sampling in the presence of phasing. There are, however, special cases where more efficient implementations are possible. In particular, we consider a linearly phased aperture, which will efficiently parameterize the general case of nonlinear phasing later on

$$F(x) = g(x) \exp(ikx \sin\theta_A) \tag{17}$$

where $g(x)$ is a real function and θ_A denotes the real tilt angle of the main radiation lobe with respect to the z axis. In this case, a more effective discretization can be obtained by Gabor expanding the real function $g(x)$ only and including the linear phasing in the beam integral (9) for the B_{m0} beam propagator. Accordingly, the narrow-waisted ($L_x \lesssim \lambda \ll d$) beam expansion can be recast as (for simplicity, the subscript "$m0$" is, henceforth, replaced by "m")

$$E_y(x, z) \approx \sum_{|m| \leq (d/2L_x)} C_m \mathcal{B}_m(x, z) \tag{18}$$

where

$$C_m = \left(L_x/\sqrt{2}\right)^{1/2} g(mL_x), \quad |m| \leq (d/2L_x) \tag{19}$$

$$\mathcal{B}_m(x, z) = -ik2^{5/4} \left(\frac{L_x}{8\pi k}\right)^{1/2} \times \exp\left\{i\left[k\left(\tilde{R}_m + mL_x \sin\theta_A + ib\right) + \pi/4\right]\right\} \times \frac{(z - ib\cos\theta_A)}{\tilde{R}_m^{3/2}} \tag{20}$$

$$\tilde{R}_m = \sqrt{(x - mL_x - ib\sin\theta_A)^2 + (z - ib\cos\theta_A)^2} \tag{21}$$

$$b = (L_x \cos\theta_A)^2/\lambda. \tag{22}$$

The beam propagator (20) differs from B_{m0} in (14) by the phase shift ($ikmL_x \sin\theta_A$) and by the different definitions of

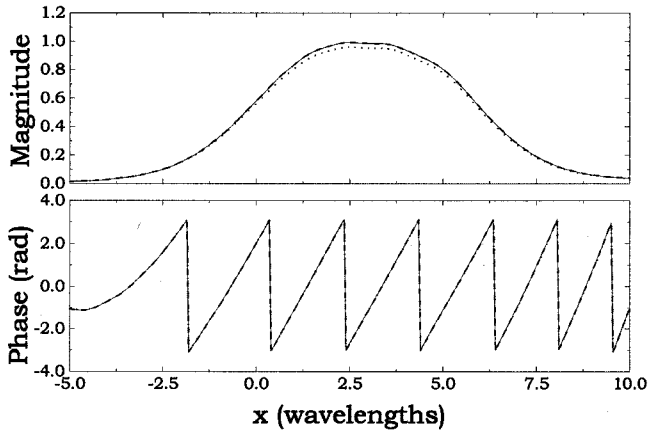

Fig. 3. Linearly phased cosine-tapered aperture distribution in (17), (23) ($d = 10\lambda$, $\theta_A = 30°$) (see Fig. 1). Near-zone ($z = 5\lambda$) radiated field synthesized using narrow-waisted nontilted and tilted beams is compared with the reference solution [Kirchhoff integration in (2)]. — Reference solution; - - - Tilted beam synthesis ($L_x = 0.02d$); · · · · · · Nontilted beam synthesis ($L_x = 0.02d$).

$\tilde{R}_m$ and b in (21), (22), respectively, which produce the propagation-matched tilt θ_A in the beam direction (see Fig. 1). For comparison of the tilted and nontilted formulations, we consider the linearly phased distribution (17) with cosine tapering

$$g(x) = \begin{cases} \cos(\pi x/d), & |x| \le d/2 \\ 0, & |x| > d/2 \end{cases} \tag{23}$$

$\theta_A = 30°$, and a fixed beam lattice period ($L_x = 0.02d$). In Fig. 3, the near-zone fields synthesized under the same conditions with the same number of narrow-waisted nontilted (13) and tilted (18) beams are compared with the reference solution [brute force Kirchhoff integration in (2)]. The tilted beam synthesis is hardly distinguishable from the reference solution, whereas the nontilted synthesis is somewhat less accurate in magnitude.

III. TD Formulation

We shall now explore the extension of the FD results for aperture radiation in Section II to time-dependent excitation, in particular to short pulses. To this end, we consider a space–time aperture field distribution at $z = 0$

$$e_y(x, z = 0, t) = f(x, t), \qquad |x| \le d/2. \tag{24}$$

Using the 2D TD Green's function [18, Sec. 7.3]

$$g_{2D}(x, z, t; x', z' = 0, t') = \frac{\mathrm{H}(t - t' - R/c)}{2\pi\sqrt{(t-t')^2 - (R/c)^2}} \tag{25}$$

with R defined in (4), c representing the speed of light, and $\mathrm{H}(\cdot)$ representing the Heaviside step function, the field radiated into the half-space $z > 0$ can be expressed via the space–time Kirchhoff integration [18], [19]

$$e_y(x, z, t) = \frac{z}{\pi}\int_{-d/2}^{d/2} dx' \, \frac{1}{R^2} \int_{-\infty}^{t-R/c} \frac{(t-t')\,\dfrac{\partial f}{\partial t'}(x', t')}{\sqrt{(t-t')^2 - (R/c)^2}}\, dt'. \tag{26}$$

It is shown in Appendix A that the FD and TD fields $E_y(x, z, \omega)$ and $e_y(x, z, t)$ in (2) and (26), respectively, are related through the Fourier transform pair

$$e_y(x, z, t) = \frac{1}{2\pi}\int_{-\infty}^{\infty} E_y(x, z, \omega)\exp(-i\omega t)\, d\omega$$
$$E_y(x, z, \omega) = \int_{-\infty}^{\infty} e_y(x, z, t)\exp(i\omega t)\, dt. \tag{27}$$

Direct numerical integration of (26) is complicated by the (integrable) square-root singularity at the upper limit $t' = t - R/c$ and requires care in its execution. Here, we use the Newton-Cotes scheme proposed in [19] for the numerical integration of (26), which represents our reference solution.

A. TD Beam Discretization: Linear-Delay Aperture Fields

The GB discretization for the time-harmonic aperture distribution in Section II can be generalized to arbitrary time-dependent excitation by use of a four-index Gabor series, which is set on a discretized lattice in the eight-dimensional (space-wavenumber, time-frequency) phase space (see [6] for analytic and computational issues). A condensed summary of the analytic results of section III-A has been given in [13], together with one simple numerical example. In our presentation below we give detailed derivations that were omitted in [13] but are required for complete understanding of the results. Moreover, we have here a much more comprehensive set of numerical examples as well as calibration of accuracy, which are not contained in [13]. The results in this section are used for the important generalization in Section III-B to nonlinear-delay profiles which is entirely new.

For assessment of the extent to which the FD narrow-waisted beam approach can be generalized to TD (short-pulse) excitation, we begin by considering the case of a space–time separable aperture field with linear time delay (assuming θ_A real)

$$f(x, t) = g(x)p\left(t - c^{-1}x\sin\theta_A\right) \tag{28}$$

and its FD counterpart via (27)

$$F(x, \omega) = P(\omega)g(x)\exp(ikx\sin\theta_A) \tag{29}$$

where $p(t)$ is a time-pulse with characteristic width T_p, and $P(\omega)$ is the Fourier transform of $p(t)$,

$$P(\omega) = \int_{-\infty}^{\infty} p(t)\exp(i\omega t)\, dt. \tag{30}$$

Equation (29) differs from (17) by the (spatially independent) frequency-dependent weight factor $P(\omega)$. This TD counterpart of the linearly phased aperture in Section II-C generates a space–time-resolved pulse propagating in the θ_A direction (see Fig. 1), with an assumed normalized pulse length much shorter than the aperture dimension d, i.e., $cT_p \ll d$.

Fourier inversion of the narrow-waisted tilted beam expansion (18) for a FD linearly phased aperture field yields a pulsed beam (PB) expansion for the corresponding TD aperture field in (28). However, the evanescent spectrum content in the FD beam propagator (20) motivates use of the *analytic signal* formulation

instead of the standard Fourier transform [5], [8]. The analytic signal $\overset{+}{f}(t)$ is defined via the one-sided Fourier transform

$$\overset{+}{f}(t) = \frac{1}{\pi}\int_0^\infty F(\omega)\exp(-i\omega t)d\omega, \qquad \mathrm{Im}(t) \le 0 \tag{31}$$

where $F(\omega)$ is the conventional Fourier spectrum of the real signal $f(t)$ [see (27)]. The real signal for real t is recovered via

$$f(t) = \mathrm{Re}\left[\overset{+}{f}(t)\right]. \tag{32}$$

The analytic TD counterpart of the narrow-waisted FD beam expansion (18) for the aperture field distribution (29) may thus be written as

$$\overset{+}{e}_y(x, z, t) \approx \sum_{|m|\le(d/2L_x)} c_m \overset{+}{\mathrm{b}}_m(x, z, t) \tag{33}$$

where the analytic PB propagator $\overset{+}{\mathrm{b}}_m$ is given in terms of the paraxial, far-zone FD propagator $\mathcal{B}_m$ in (20)

$$\overset{+}{\mathrm{b}}_m(x, z, t) = \frac{1}{\pi}\int_0^\infty \mathcal{B}_m(x, z, \omega)P(\omega) \times \exp(-i\omega t)d\omega \qquad \mathrm{Im}(t) \le 0. \tag{34}$$

For implementation, one can choose a frequency-independent beam lattice period L_x (resulting in a frequency (i.e., wavelength)-dependent beam parameter b [see (22)], or a frequency-independent beam parameter b (resulting in a frequency-dependent L_x). We consider frequency-independent L_x preferable because this yields frequency-independent Gabor coefficients [see (19)]. The real TD field e_y then follows from (33) and (34)

$$e_y(x, z, t) = \mathrm{Re}\left[\overset{+}{e}_y(x, z, t)\right]$$

with

$$\mathrm{b}_m(x, z, t) = \mathrm{Re}\left[\overset{+}{\mathrm{b}}_m(x, z, t)\right] \tag{35}$$

where the Gabor coefficients c_m can be estimated through aperture sampling when $L_x \lesssim \lambda \ll d$ [see (19)]

$$c_m = \left(L_x/\sqrt{2}\right)^{1/2} g(mL_x), \qquad |m| \le (d/2L_x). \tag{36}$$

For the important class of Gaussian time pulses, we have found useful closed-form approximations for the integral in (34). In particular, we use a Rayleigh (four-times-differentiated Gaussian) pulse (see Fig. 4)

$$p(t) = \exp\left[-\frac{50(t-T_p/2)^2}{T_p^2}\right] \times \left[1 + \frac{10\,000(t-T_p/2)^4 - 600(t-T_p/2)^2T_p^2}{3T_p^4}\right] \tag{37}$$

with spectrum

$$P(\omega) = \sqrt{\frac{\pi}{2}}\,\frac{\omega^4 T_p^5}{150\,000}\exp\left(-\frac{\omega^2T_p^2}{200} + i\,\frac{\omega T_p}{2}\right) \tag{38}$$

which has desirable wideband properties, being sufficiently bounded away from $\omega = 0$ and ∞. However, the procedure below can be applied to any kind of modulated or differentiated Gaussian pulse.

The beam parameter b and hence, the complex distance $\tilde{R}_m$ (21) in (20) are *frequency dependent* because the beam lattice period L_x has been chosen frequency independent. For $z \gg |b\cos\theta_A|$, the amplitude factor in the FD beam propagator (20) can be approximated by

$$\frac{(z - ib\cos\theta_A)}{\tilde{R}_m^{3/2}} \approx \frac{z}{R_m^{3/2}} \qquad R_m = \sqrt{(x-mL_x)^2 + z^2} \tag{39}$$

where the distance $R_m \approx \tilde{R}_m$ is *real* and frequency independent. In the phase, under the same conditions, we retain the first order paraxial correction

$$\tilde{R}_m \approx z_{bm} - ib + \frac{x_{bm}^2}{2(z_{bm} - ib)} \approx z_{bm} - ib + \frac{x_{bm}^2(z_{bm} + ib)}{2z_{bm}^2}, \qquad b \ll z_{bm} \tag{40}$$

where (x_{bm}, z_{bm}) are the beam coordinates (see Fig. 1)

$$\begin{bmatrix} x_{bm} \\ z_{bm} \end{bmatrix} = \begin{bmatrix} \cos\theta_A & -\sin\theta_A \\ \sin\theta_A & \cos\theta_A \end{bmatrix}\begin{bmatrix} x - mL_x \\ z \end{bmatrix}. \tag{41}$$

The phase approximation (40) is valid in the paraxial region of each beam

$$|z_{bm} - ib| \gg |x_{bm}| \tag{42}$$

together with the constraint that the beam parameter b remains small over the bandwidth Ω_p of the pulse spectrum $P(\omega)$

$$b = \frac{(L_x\cos\theta_A)^2\omega}{2\pi c} \ll z_{bm}, \qquad \omega \le \Omega_p. \tag{43}$$

With these approximations, the integral in (34) can be evaluated in closed form, and the analytic PB propagator can written explicitly as (see Appendix B for details)

$$\overset{+}{\mathrm{b}}_m(x, z, t) \approx \eta_m\left[\alpha_m\Gamma\left(\frac{11}{4}\right)\mathrm{M}_1\left(5\sqrt{\frac{\pi}{2}}\,\frac{\beta_m}{\alpha_m}\right) + 5\sqrt{2\pi}i\beta_m\Gamma\left(\frac{13}{4}\right)\mathrm{M}_2\left(5\sqrt{\frac{\pi}{2}}\,\frac{\beta_m}{\alpha_m}\right)\right] \tag{44}$$

with

$$\alpha_m(x, z) = \sqrt{\pi(cT_pz_{bm})^2 + 50(L_xx_{bm}\cos\theta_A)^2} \tag{45}$$

$$\beta_m(x, z, t) = x_{bm}^2 + z_{bm}(2z_{bm} + cT_p - 2ct) + 2mL_xz_{bm}\sin\theta_A \tag{46}$$

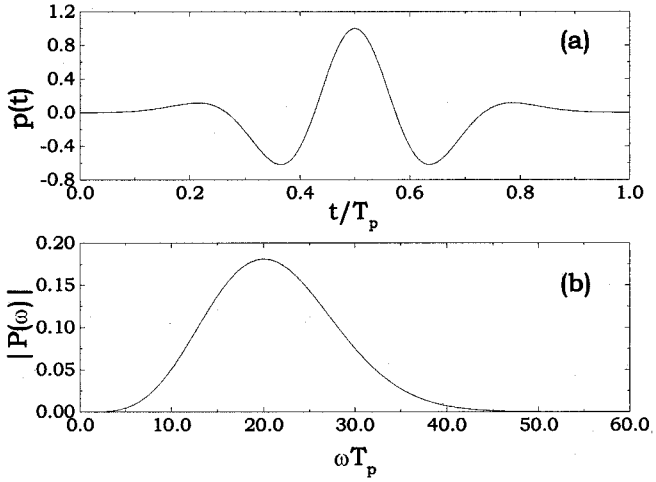

Fig. 4. Rayleigh pulse. (a) Temporal profile in (37). (b) Spectrum (magnitude) in (38).

$$\eta_m(x,\,z)=\frac{4z\sqrt{10L_x}\pi^{7/4}(cT_p)^5 z_{bm}^{11/2}\exp(-i\pi/4)}{3R_m^{3/2}\alpha_m(x,\,z)^{13/2}} \tag{47}$$

$$\mathrm{M}_1(y)={}_1\mathrm{F}_1\left(\tfrac{11}{4},\,\tfrac{1}{2},\,-y^2\right) \tag{48}$$

$$\mathrm{M}_2(y)={}_1\mathrm{F}_1\left(\tfrac{13}{4},\,\tfrac{3}{2},\,-y^2\right) \tag{49}$$

where R_m, x_{bm} and z_{bm} are defined in (39) and (41), $\Gamma(\cdot)$ is the gamma function [20, Sec. 6], and ${}_1\mathrm{F}_1(u,\,v,\,y)$ is the Kummer confluent hypergeometric function [20, Sec. 13]. Since modulation or differentiation operations affect only the arguments of ${}_1\mathrm{F}_1(u,\,v,\,y)$, the above reduction can be applied to *any* Gaussian-envelope pulse.

The following simple approximations can be exploited for the functions M_1 and M_2 (see Appendix C):

$$\mathrm{M}_1(y)\approx\exp(-y^2)\left(1-\frac{9}{2}\,y^2+\frac{15}{8}\,y^4-\frac{y^6}{16}-\frac{3}{896}\,y^8-\frac{y^{10}}{3840}\right) \tag{50}$$

$$\mathrm{M}_2(y)\approx\exp(-y^2)\left(1-\frac{7}{6}\,y^2+\frac{7}{40}\,y^4+\frac{y^6}{240}+\frac{y^8}{3456}+\frac{y^{10}}{42\,240}\right). \tag{51}$$

Fig. 5 shows comparisons between the exact functions (computed via reliable numerical routines [21]) and the proposed approximations (50), (51). The results essentially overlap on the scale of the plots. Since the functions $\mathrm{M}_{1,\,2}$ resemble the form and shape of the Rayleigh pulse in (37) and Fig. 4, then using (50) and (51), the TD beam propagator (44) can be computed very efficiently. Fig. 6 shows a number of instantaneous snapshots of $\mathtt{b}_m(x,\,z,\,t)$. Note the rapid transverse spatial spreading of the ray-like narrow-waisted PB, but its retention of the wavefront behavior in the longitudinal (radial) direction.

B. TD Beam Discretization: Nonlinear-Delay Aperture Fields

Extension of the TD Gabor algorithm in Section III-A to nonlinear delay profiles is an important new generalization. Instead

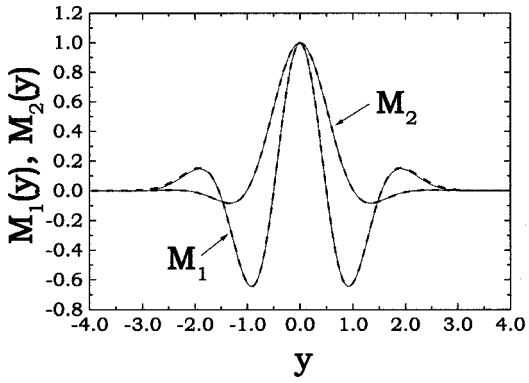

Fig. 5. Comparison between the exact and approximated functions $\mathrm{M}_{1,\,2}$ in (48)–(51). — Exact; - - - Approximated.

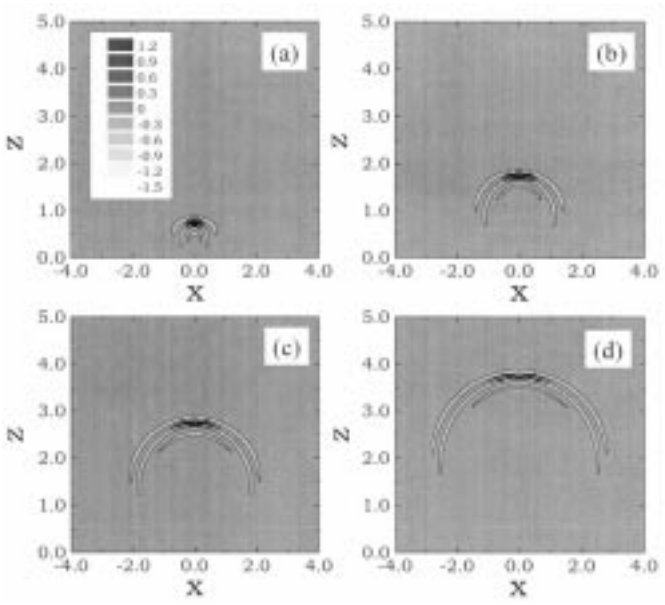

Fig. 6. Instantaneous snapshots of the TD beam propagator $\mathtt{b}_m(x,\,z,\,t)$ ($m=0$, $L_x=d/20$, $\theta_A=0$, $cT_p=0.5$). (a) $ct=1$. (b) $ct=2$. (c) $ct=3$. (d) $ct=4$.

of the linear delay in (28), we now consider the aperture field distribution

$$f(x,\,t)=h(x)p\left(t-c^{-1}\phi(x)\right) \tag{52}$$

with its FD counterpart

$$F(x,\,\omega)=P(\omega)h(x)\exp\left[i\,\frac{\omega}{c}\,\phi(x)\right] \tag{53}$$

where $h(x)$ and $\phi(x)$ are real functions. Recalling the efficient treatment of the linear delay fields in Section III-A, we split the phase (delay) function $\phi(x)$ into a linear part plus a nonlinear remainder

$$\phi(x)=x\sin\theta_A+\phi_{NL}(x) \tag{54}$$

where $\phi_{NL}(x)$ does not contain linear terms. The FD narrow-waisted tilted beam decomposition (18) of Section II-C can, thus, be applied, with $g(x)$ in (17) given by

$$g(x)=h(x)\exp[ik\phi_{NL}(x)]. \tag{55}$$

The corresponding FD Gabor coefficients [see (19)] are complex

$$C_m = \left(L_x/\sqrt{2}\right)^{1/2} h(mL_x)\exp[ik\phi_{NL}(mL_x)] \qquad |m| \le (d/2L_x) \tag{56}$$

and the corresponding TD beam expansion differs only slightly from (33)

$$e_y(x,\, z,\, t) \approx \sum_{|m|\le(d/2L_x)} h_m \mathsf{b}_m(x,\, z,\, t-\tau_m) \tag{57}$$

where b_m is the real part of the analytic PB propagator in (44), and

$$h_m = \left(L_x/\sqrt{2}\right)^{1/2} h(mL_x)$$
$$\tau_m = c^{-1}\phi_{NL}(mL_x), \qquad |m| \le (d/2L_x). \tag{58}$$

C. Assessment of Accuracy

The explicit analytic results in (44) are based on the approximations (39) and (40), which are valid in the paraxial *far-zone* (42). An additional condition is the *smallness* of the beam parameter b over the whole bandwidth of interest [see (43)]. This latter restriction, in turn, determines the maximum allowable lattice period (i.e., the minimum number of beams) for specified Ω_p, θ_A and observation point. A rough theoretical estimate can be obtained from (43). For specified observation plane at $z = z_{obs}$ and recalling that $z_{bm} = z_{obs}/\cos\theta_A$ (see Fig. 1) the overall constraint can be expressed by the following inequality in terms of the nondimensional estimator Q

$$Q \equiv N_b^{-1}\sqrt{\frac{\kappa(\cos\theta_A)^3}{\chi}} \ll 1 \tag{59}$$

where the integer $N_b = d/L_x$ represents the number of beams in the expansion (33), $\kappa = \Omega_p T_p/2\pi$ is the normalized bandwidth of the pulse $p(t)$, and $\chi = z_{obs}/F_d$ is the distance to the observation plane scaled by the Fresnel distance of the aperture, $F_d = d^2/(cT_p)$. The nondimensional estimator $Q \ll 1$ contains all relevant parameters of the problem. For example, decreasing the number of beams N_b can be compensated by a corresponding increase of $(z_{obs})^{1/2}$. However, a finer discretization may be required in the presence of nonlinear phasing/delay for the same degree of accuracy.

D. Numerical Results

The TD narrow-waisted beam expansions in (35), (57) have been calibrated against a reference solution implemented by space–time Kirchhoff integration of (26) in an extensive number of numerical simulations. We present and discuss selected typical results, starting with the linear-delay space–time aperture distribution (28) where $g(x)$ is the cosine tapering in (23) and $p(t)$ is the time dependence of the Rayleigh pulse in (37). Figs. 7 and 8 show typical results for the nonphased case ($\theta_A = 0$). Specifically, Fig. 7(a) depicts the time evolution of the y-directed scalar electric field at a fixed observation point in the near zone ($z = 0.1F_d$) of a large aperture ($d = 10cT_p$); the reference space–time Kirchhoff integration (26) is compared with the TD beam synthesis (35) for various numbers of beams. In all simulations, we used a pulse-bandwidth value $\Omega_p T_p = 40$ (see

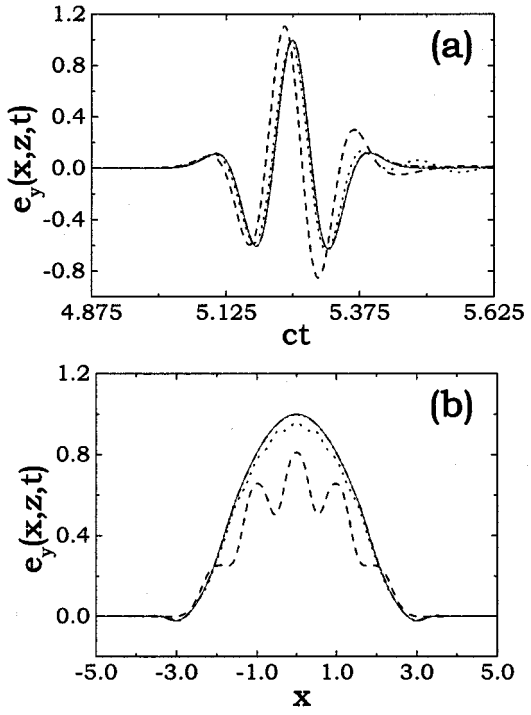

Fig. 7. Radiated field due to nonphased ($\theta_A = 0$) cosine-tapered aperture distribution. Parameters: $cT_p = 0.5$, $d = 5 = 10cT_p$ (arbitrary units). Reference solution via space–time Kirchhoff integration of (26): solid curves. TD narrow-waisted beam synthesis in (35): dashed and dotted curves. Observation points for the temporal profile are on the beam axis ($x = 0$). (a) Temporal profile at $x = 0$, $z = 5 = 0.1F_d$ (arbitrary units); (b) Spatial transverse profile at $z = 5$, $ct = 5.25$; - - - 5 beams ($Q = 1.6$, $\Delta e_y = -2$ dB); $\cdots\cdots$ 10 beams ($Q = 0.8$, $\Delta e_y = -14$ dB), - · - · - 30 beams ($Q = 0.26$, $\Delta e_y = -31$ dB). The r.m.s. errors Δe_y pertain to Fig. 7(a).

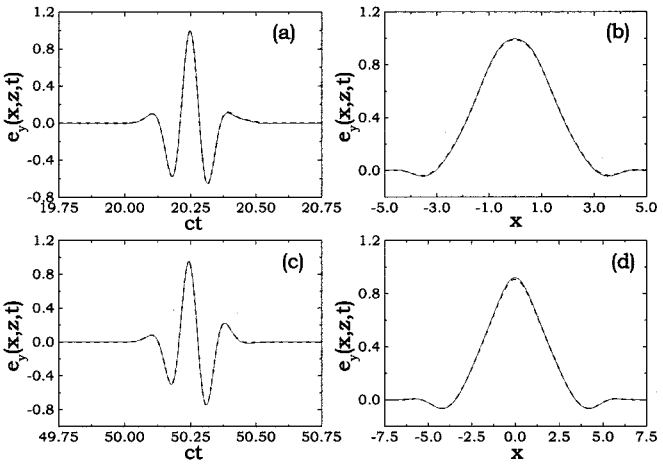

Fig. 8. Parameters as in Fig. 7. (a) Temporal profile at $x = 0$, $z = 20 = 0.4F_d$, 15 beams ($Q = 0.27$, $\Delta e_y = -32$ dB). (b) Spatial transverse profile at $z = 20$, $ct = 20.25$, 15 beams ($Q = 0.27$). (c) Temporal profile at $x = 0$, $z = 50 = F_d$, 10 beams ($Q = 0.25$, $\Delta e_y = -34$ dB). (d) Spatial transverse profile at $z = 50$, $ct = 50.25$, 10 beams ($Q = 0.25$). Reference solutions (solid curves) and beam solutions (dashed curves) coincide on the scale of the plots.

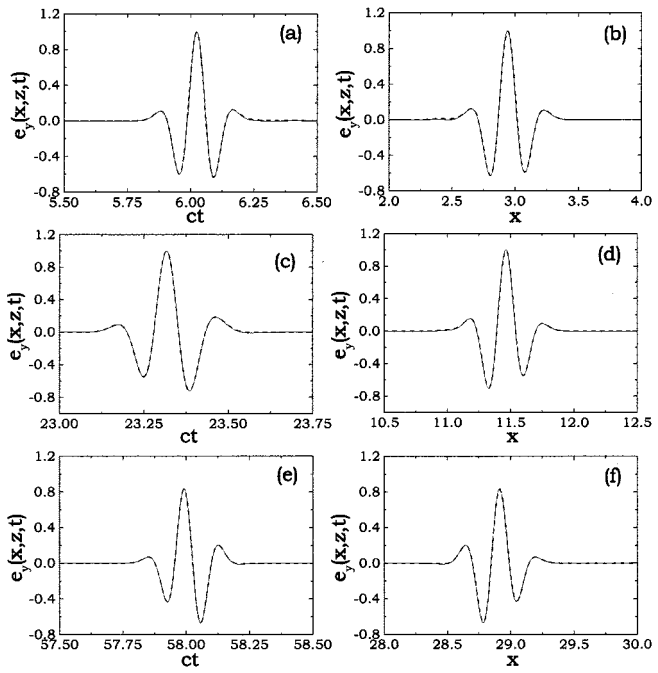

Fig. 9. Radiated field due to linearly phased ($\theta_A = 30°$) cosine-tapered aperture distribution. Parameters: $cT_p = 0.5$, $d = 5 = 10cT_p$ (arbitrary units). Observation points for the temporal profiles are on the tilted beam axis θ_A. (a) Temporal profile at $x = 2.89$, $z = 5 = 0.1F_d$ (arbitrary units), 25 beams ($Q = 0.26$, $\Delta e_y = -32$ dB). (b) Spatial transverse profile at $z = 5$, $ct = 6.05$, 25 beams ($Q = 0.26$). (c) Temporal profile at $x = 11.5$, $z = 20 = 0.4F_d$, 12 beams ($Q = 0.27$, $\Delta e_y = -33$ dB). (d) Spatial transverse profile at $z = 20$, $ct = 23.3$, 12 beams ($Q = 0.27$). (e) Temporal profile at $x = 28.9$, $z = 50 = F_d$, 8 beams ($Q = 0.25$, $\Delta e_y = -33$ dB). (f) Spatial transverse profile at $z = 50$, $ct = 58$, 8 beams ($Q = 0.25$). Reference solutions (solid curves) and beam solutions (dashed curves) coincide on the scale of the plots.

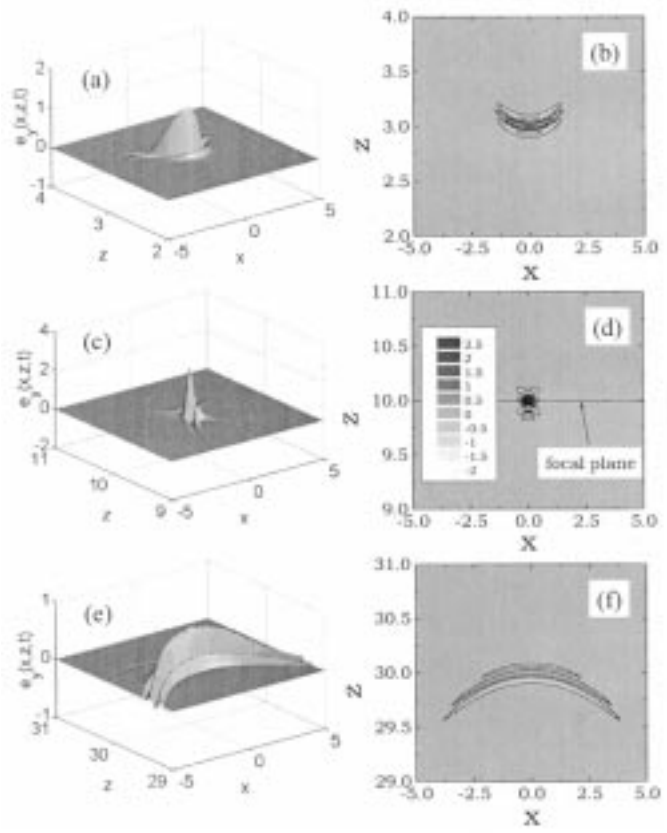

Fig. 10. Radiated field due to cosine-tapered focused aperture distribution in (61), computed via space–time Kirchhoff integration of (26). Parameters: $cT_p = 0.5$, $d = 5 = 10cT_p$, $L_f = 10 = 0.2F_d$ (arbitrary units). Instantaneous snapshots at various times. (a) $ct = 3.25$; (c) $ct = 10.235$; (e) $ct = 30.22$. (b), (d), (f) Gray-scale plots corresponding to (a), (c), (e), respectively. See also the spatial profiles in Figs. 12(b), 11(b) and 12(d) for different visualization.

Fig. 4), which sets the reference level for the nondimensional estimator Q in (59). As expected, the agreement improves with increase in the number of beams, and satisfactory accuracy is achieved for $Q \leq 0.3$. In order to better quantify the accuracy of the TD beam synthesis and the role of the nondimensional estimator Q, we computed the r.m.s. (energy) error at a fixed observation point

$$\Delta e_y := \frac{\displaystyle\int_{-\infty}^{\infty} \left| e_y^{(\mathrm{ref})}(x,z,t) - e_y^{(\mathrm{beam})}(x,z,t) \right|^2 dt}{\left[\displaystyle\int_{-\infty}^{\infty} \left| e_y^{(\mathrm{ref})}(x,z,t) \right|^2 dt \int_{-\infty}^{\infty} \left| e_y^{(\mathrm{beam})}(x,z,t) \right|^2 dt \right]^{1/2}} \tag{60}$$

whose values are explicitly indicated in the figure captions. It is observed that values of $Q \leq 0.3$ yield errors $\lesssim -30$ dB. We shall use Q as a convenient calibrator of the accuracy in the numerical experiments. It is observed from the transverse cut shown in Fig. 7(b) that despite the use of the paraxial far-zone approximation (42), the TD beam synthesis works quite well even in the near zone of the aperture ($z = 0.1F_d$) and not only around the main radiation lobe. As the observation distance increases, a coarser discretization can be used subject to (59). For instance, Fig. 8(a) and (b) show results for a moderate observation distance ($z = 0.4F_d$), whereas Fig. 8(c) and (d) show far-zone ($z = F_d$) results. In these examples, only one beam synthesis is shown, with the beam lattice period chosen so as to assure $Q \leq 0.3$, according to the above calibration; accuracy is confirmed. We conclude that even at moderate distances, acceptable results can be obtained with a relatively small number of beams (∼20). The corresponding data for a linear-delay example ($\theta_A = 30°$) are shown in Fig. 9. The same conclusions apply, except that the field maxima are tracked along the tilted beam axis θ_A.

As our final and most important example, we consider a nonlinearly phased aperture distribution. In particular, we have chosen a cosine-tapered aperture field with quadratic delay

$$f(x,t) = \begin{cases} \cos(\pi x/d)p[t + x^2/(2cL_f)], & |x| \leq d/2 \\ 0, & |x| > d/2 \end{cases} \tag{61}$$

which represents the TD counterpart of a typical time-harmonic focusing ($L_f > 0$) or defocusing ($L_f < 0$) distribution, with L_f representing the conventional focal length. The focusing case is the most challenging, since standard (nonuniform) ray asymptotics would fail due to the presence of caustic transition regions. Moreover, we have chosen numerical values so as to get focusing at moderate distance from the aperture ($L_f = 0.2F_d$). A

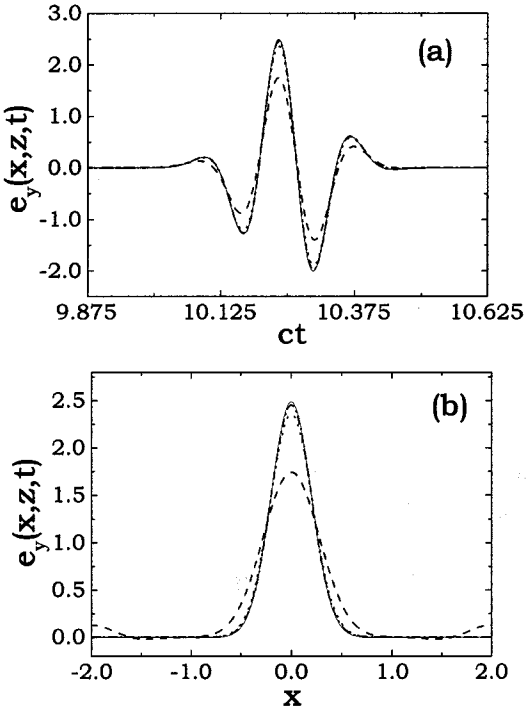

Fig. 11. Radiated field due to cosine-tapered focused aperture distribution in (61), observed in the focal plane. Parameters: $cT_p = 0.5$, $d = 5 = 10cT_p$, $L_f = 10 = 0.2F_d$ (arbitrary units). Reference solution via space–time Kirchhoff integration of (26): solid curves. TD narrow-waisted beam synthesis in (57): dashed and dotted curves. (a) Temporal profile at $x = 0$, $z = 10 = L_f = 0.2F_d$. (b) Spatial transverse profile at $z = 10$, $ct = 10.235$; - - - 10 beams ($Q = 0.56$, $\Delta e_y = -9$ dB), $\cdots\cdots$ 30 beams ($Q = 0.19$, $\Delta e_y = -25$ dB), - · - · - 60 beams ($Q = 0.09$, $\Delta e_y = -33$ dB). The r.m.s. errors Δe_y pertain to Fig. 11(a).

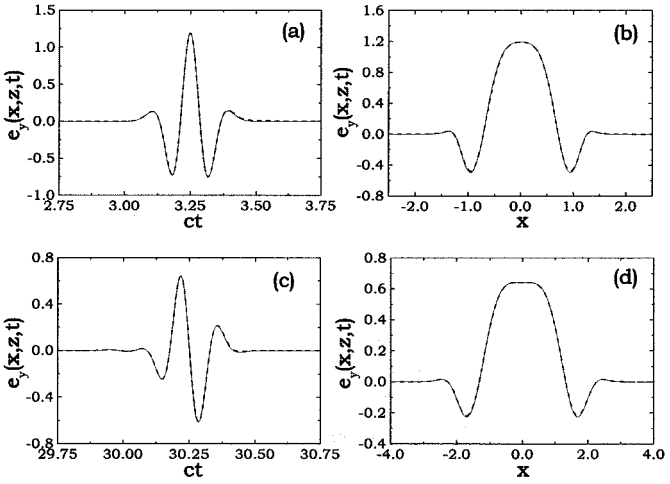

Fig. 12. Parameters as in Fig. 11, observed before and beyond the focal plane. (a) Temporal profile at $x = 0$, $z = 3 = 0.3L_f = 0.06F_d$, 100 beams ($Q = 0.1$, $\Delta e_y = -33$ dB); (b) Spatial transverse profile at $z = 3$, $ct = 3.25$, 100 beams ($Q = 0.1$); (c) Temporal profile at $x = 0$, $z = 30 = 3L_f = 0.6F_d$, 30 beams ($Q = 0.1$, $\Delta e_y = -37$ dB); (d) Spatial transverse profile at $z = 30$, $ct = 30.22$, 30 beams ($Q = 0.1$). Reference solutions (solid curves) and beam solutions (dashed curves) coincide on the scale of the plots.

sequence of instantaneous snapshots of the radiated field at different times, computed via the space–time Kirchhoff integration in (26), is shown in Fig. 10. One observes how the space–time wavepacket, starting from the initial distribution (61), has a concave (focusing) wavefront on its way to the focal plane, i.e., for $z < L_f$ [Fig. 10(a) and (b)]; it experiences its maximum space–time localization at the focal plane $z = L_f$ [Fig. 10(c) and (d)], and spreads out beyond the focal plane with a convex wavefront [Fig. 10(e) and (f)]. In order to assess the accuracy of the PB expansion in (57), the comparison with the reference solution is shown in Figs. 11 and 12 for representative temporal and spatial cuts at various observation distances. Fig. 11(a) and (b) show the convergence results at the focal plane $z = L_f$ (most challenging test). A slightly finer discretization is needed than in the linear-delay case, for the same degree of accuracy; accurate syntheses ($\Delta e_y < -30$ dB) are obtained for $Q \leq 0.1$, but reasonable accuracy ($\Delta e_y < -20$ dB) is still within the less stringent $Q \leq 0.3$ range. Fig. 12(a)–(d), show results for observation distances smaller ($z = 0.3L_f$) and larger ($z = 3L_f$) than the focal length, with the number of beams chosen so as to assure $Q \leq 0.1$. The spatial profiles in Fig. 12(b) and (d) show the broader spatial extent of the wavefront, with respect to the focal plane pattern in Fig. 11(b), which is analogous to the snapshots in Fig. 10(a) and (e). The temporal profile of the incident pulse in Fig. 12(a) is distorted at [Fig. 11(a)] and beyond [Fig. 12(c)] the focus due to caustic-induced phase shifts.

IV. Conclusion

By extending the time-harmonic approach presented in [1], a 2D narrow-waisted pulsed beam algorithm has been presented which allows an effective discretization of short-pulse radiation from one-dimensional (1-D) large apertures. Analytic approximations in the form of readily computable functions have been obtained for aperture field distributions with separable space–time dependence, general phasing, and Gaussian pulse excitation.

Accuracy assessments of the beam algorithm have been formalized theoretically in terms of the nondimensional estimator Q, and calibrated numerically through a variety of simulations involving phased and focused pulsed aperture field profiles; independent calibration of the numerical data was achieved by comparison with a rigorously based brute force space–time Kirchhoff integration. The results are encouraging and confirm that within the stated criteria, one can make fairly reliable predictions of performance.

Overall, it appears that reasonably accurate syntheses can be obtained with a moderate number of beams, within the constraint $Q \leq 0.3$, thus making the algorithm a promising efficient parameterizer for beam tracing in the presence of propagation and scattering environments. Toward this goal, the TD extension of the previously performed FD studies in [11]–[14] is now under consideration [22]. For extension to two-dimensional (2-D) apertures which generate three-dimensional (3-D) (vector) fields, see [23].

Appendix A
Pertaining to (26)

By Fourier transforming the FD radiated field in (2), recalling that G_{2D} and g_{2D} are related through the Fourier transform pair

(27) [18], and applying the convolution theorem [24], the TD field radiated into the $z > 0$ halfspace can be written as

$$e_y(x, z, t) = -\frac{1}{\pi}\int_{-d/2}^{d/2} dx' \frac{\partial}{\partial z}\int_{-\infty}^{t-R/c} \times \frac{f(x', t')}{\sqrt{(t-t')^2 - (R/c)^2}}\, dt' \qquad (62)$$

with R being defined in (4), and with $f(x, t)$ and $F(x, \omega)$ being related through the Fourier transform pair (27). The differentiation of the temporal integral in (62) can be performed through differentiation under the integral sign, coupled with a limiting procedure to circumvent the singularity at the upper integration limit (see [19] for details), yielding

$$\frac{\partial}{\partial z}\int_{-\infty}^{t-R/c} \frac{f(x', t')}{\sqrt{(t-t')^2 - (R/c)^2}}\, dt' = -\frac{z}{R^2}\int_{-\infty}^{t-R/c} \frac{(t-t')\dfrac{\partial f}{\partial t'}(x', t')}{\sqrt{(t-t')^2 - (R/c)^2}}\, dt' \qquad (63)$$

from which (26) follows.

Appendix B
Pertaining to (44)

By substituting (20) and (38), with (22), (39), (40), into (34) one obtains

$$\overset{+}{\mathrm{b}}_m(x, z, t) = -\frac{2^{-3/4} e^{i3\pi/4}\sqrt{L_x} z T_p^5}{150000\pi\sqrt{c} R_m^{3/2}} \int_0^\infty \omega^{9/2} \times \exp\left[i\omega\left(\frac{i\alpha_m^2\omega + 100\pi c z_{bm}\beta_m}{200c^2\pi z_{bm}^2}\right)\right] d\omega \qquad (64)$$

with α_m, β_m defined in (45), (46), respectively. The frequency integral in (64), in its canonical form

$$I(\xi, \zeta) = \int_0^\infty \omega^{9/2} \exp\left(i\xi\omega - \zeta\omega^2\right) d\omega, \qquad \zeta > 0 \qquad (65)$$

can be evaluated in closed form (we used Mathematica [21]) as

$$I(\xi, \zeta) = \frac{\zeta^{-13/4}}{2}\left[\sqrt{\zeta}\,\Gamma\left(\frac{11}{4}\right){}_1\mathrm{F}_1\left(\frac{11}{4}, \frac{1}{2}, -\frac{\xi^2}{4\zeta}\right) + i\xi\,\Gamma\left(\frac{13}{4}\right){}_1\mathrm{F}_1\left(\frac{13}{4}, \frac{3}{2}, -\frac{\xi^2}{4\zeta}\right)\right] \qquad (66)$$

where $\Gamma(\cdot)$ is the gamma function [20, Sec. 6], and ${}_1\mathrm{F}_1(u, v, y)$ is the Kummer confluent hypergeometric function [20, Sec. 13]. Equation (44) follows from (64), (66) after straightforward algebra.

Appendix C
Pertaining to (50), (51)

The Kummer confluent hypergeometric function is defined as [20, Sec. 13]

$${}_1\mathrm{F}_1(u, v, y) = \sum_{n=0}^{\infty} \frac{(u)_n y^n}{(v)_n n!} \qquad (67)$$

where $(u)_n$ is the Pochammer symbol [20]

$$(u)_n = u(u+1)(u+2)\cdots(u+n-1) \qquad (u)_0 = 1. \qquad (68)$$

A rapidly convergent approximation for the functions M_1 and M_2 in (48), (49) can be obtained by exploiting the Kummer transformation [20]

$${}_1\mathrm{F}_1(u, v, y) = \exp(y){}_1\mathrm{F}_1(v-u, v, -y). \qquad (69)$$

Accordingly

$$\begin{aligned}\mathrm{M}_1(y) &= {}_1\mathrm{F}_1\left(\tfrac{11}{4}, \tfrac{1}{2}, -y^2\right) \\ &= \exp\left(-y^2\right){}_1\mathrm{F}_1\left(-\tfrac{9}{4}, \tfrac{1}{2}, y^2\right) \\ &= \exp\left(-y^2\right)\left(1 - \frac{9}{2}y^2 + \frac{15}{8}y^4 - \frac{y^6}{16} - \frac{3}{896}y^8 - \frac{y^{10}}{3840} + \mathcal{O}\left(y^{12}\right)\right) \qquad (70)\end{aligned}$$

$$\begin{aligned}\mathrm{M}_2(y) &= {}_1\mathrm{F}_1\left(\tfrac{13}{4}, \tfrac{3}{2}, -y^2\right) \\ &= \exp\left(-y^2\right){}_1\mathrm{F}_1\left(-\tfrac{7}{4}, \tfrac{3}{2}, y^2\right) \\ &= \exp\left(-y^2\right)\left(1 - \frac{7}{6}y^2 + \frac{7}{40}y^4 + \frac{y^6}{240} + \frac{y^8}{3456} + \frac{y^{10}}{42240} + \mathcal{O}\left(y^{12}\right)\right) \qquad (71)\end{aligned}$$

as shown in (50) and (51).

References

[1] J. J. Maciel and L. B. Felsen, "Systematic study of fields due to extended apertures by Gaussian beam discretization," *IEEE Trans. Antennas Propagat.*, vol. 37, pp. 884–892, July 1989.

[2] P. D. Einziger and M. Shapira, "Gabor representation and aperture theory," *J. Opt. Soc. Amer. A*, vol. 3, no. 4, pp. 508–522, Apr. 1986.

[3] B. Z. Steinberg, H. Heyman, and L. B. Felsen, "Phase-space beam summation for time-harmonic radiation from large apertures," *J. Opt. Soc. Amer. A*, vol. 8, no. 1, pp. 41–59, Jan. 1991.

[4] ——, "Phase-space methods for radiation from large apertures," *Radio Sci.*, vol. 26, no. 1, pp. 219–227, Jan.–Feb. 1991.

[5] B. Z. Steinberg and E. Heyman, "Phase-space beam summation for time-dependent radiation from large apertures: Continuous parameterization," *J. Opt. Soc. Amer. A*, vol. 8, no. 6, pp. 943–958, June 1991.

[6] ——, "Phase-space beam summation for time-dependent radiation from large apertures: Discretized parameterization," *J. Opt. Soc. Am. A*, vol. 8, no. 6, pp. 959–966, June 1991.

[7] B. Rao and L. Carin, "A hybrid (parabolic equation)-(Gaussian beam) algorithm for wave propagation through large inhomogeneous regions," *IEEE Trans. Antennas Propagat.*, vol. 46, pp. 700–709, May 1998.

[8] E. Heyman and T. Melamed, "Space–time representation of ultra wideband signals," in *Advances in Imaging and Electron Physics*, P. W. Hawkes, Ed. New York: Academic Press, 1998, vol. 103, pp. 1–63.

[9] T. Melamed, E. Heyman, and L. B. Felsen, "Local spectral analysis of short-pulse excited scattering from weakly inhomogeneous media. Part I: Forward scattering," *IEEE Trans. Antennas Propagat.*, vol. 47, pp. 1208–1217, July 1999.

[10] B. Rao and L. Carin, "Beam-tracing-based inverse scattering for general aperture antennas," *J. Opt. Soc. Am. A*, vol. 16, no. 9, pp. 2219–2231, Sept. 1999.

[11] J. J. Maciel and L. B. Felsen, "Gaussian beam analysis of propagation from an extended aperture distribution through dielectric layers, Part I—Plane layer," *IEEE Trans. Antennas Propagat.*, vol. 38, pp. 1607–1617, Oct. 1990.
[12] ——, "Gaussian beam analysis of propagation from an extended aperture distribution through dielectric layers, Part II—Circular cylindrical layer," *IEEE Trans. Antennas Propagat.*, vol. 38, pp. 1618–1624, Oct. 1990.
[13] L. B. Felsen and V. Galdi, "Complex-source-point narrow-waisted ray-like Gaussian beams for frequency and time domain radiation and scattering," in *Ultra-Wideband, Short Pulse Electromagnetics 5*, S. R. Cloude and P. D. Smith, Eds, NY: Kluwer/Plenum, 2001.
[14] V. Galdi, L. B. Felsen, and D. A. Castañon, "Quasi-ray Gaussian beam algorithm for time-harmonic two-dimensional scattering by moderately rough interfaces," *IEEE Trans. Antennas Propagat.*, vol. 49, pp. 1305–1314, Sept. 2001.
[15] V. Galdi, D. A. Castañon, and L. B. Felsen, "Multifrequency reconstruction of moderately rough interfaces via quasi-ray Gaussian beams," IEEE Trans. Geosci. Remote Sensing, Sept. 2000, submitted for publication.
[16] M. J. Bastiaans, "Gabor's expansion of a signal into Gaussian elementary signals," *Proc. IEEE*, vol. 68, pp. 538–539, Apr. 1980.
[17] ——, "A sampling theorem for the complex spectrogram, and Gabor's expansion of a signal in Gaussian elementary signals," *Opt. Eng.*, vol. 20, pp. 594–598, 1981.
[18] P. M. Morse and H. Feshbach, *Methods of Theoretical Physics*. New York: McGraw-Hill, 1953.
[19] M. Kragalott, M. S. Kluskens, and W. P. Pala, "Time-domain fields exterior to a two-dimensional FDTD space," *IEEE Trans. Antennas Propagat.*, vol. 45, pp. 1655–1663, Nov. 1997.
[20] M. Abramowitz and I. A. Stegun, *Handbook of Mathematical Functions*. New York: Dover, 1964.
[21] S. Wolfram, *The Mathematica Book*, 3rd ed. Cambridge, U.K.: Cambridge Univ. Press, 1996.
[22] V. Galdi, L. B. Felsen, and D. A. Castañon, "Quasi-ray Gaussian beam algorithm for short-pulse two-dimensional scattering by moderately rough interfaces," IEEE Trans. Antennas Propagat., Feb. 2001, submitted for publication.
[23] ——, "Time-domain radiation from large two-dimensional apertures via narrow-waisted Gaussian beams," IEEE Trans. Antennas Propagat., Jan. 2001, submitted for publication.
[24] A. Papoulis, *Signal Analysis*. New York: McGraw-Hill, 1977.

Vincenzo Galdi (M'98) was born in Salerno, Italy, on July 28, 1970. He received the Laurea degree *(summa cum laude)* in electrical engineering and the Ph.D. degree in applied electromagnetics from the University of Salerno, Italy, in 1995 and 1999, respectively.

From April to December 1997, he held a Visiting Position in the Radio Frequency Division of the European Space Research & Technology Centre (ESTEC-ESA), Noordwijk, The Netherlands, where he was involved in developing CAD tools for microwave filters and phased-array antennas with coaxial excitation. In September 1999, he received a European Union postdoctoral fellowship through the University of Sannio, Benevento, Italy. In October 1999, he became a Research Associate in the Department of Electrical and Computer Engineering, Boston University, Boston, MA, where he is currently working on wave-oriented imaging algorithms for landmine detection and classification. His research interests include analytical and numerical techniques for wave propagation in complex environments, path integrals, and stochastic resonance.

Dr. Galdi is the recipient of the 2001 International Union of Radio Science (URSI) "Young Scientist Award." He is a member of Sigma Xi.

Leopold B. Felsen (S'47–M'54–SM'55–F'62–LF'90) was born in Munich, Germany, on May 7, 1924. He received the B.E.E., M.E.E, and D.E.E. degrees from the Polytechnic Institute of Brooklyn, Brooklyn, NY, in 1948, 1950, and, 1952, respectively.

He emigrated to the United States in 1939 and served in the U.S. Army from 1943 to 1946. After 1952, he remained with the Polytechnic Institute of Brooklyn (now Polytechnic University), becoming a Professor in 1962 and University Professor in 1978. From 1974 to 1978, he was Dean of Engineering. In 1994, he resigned from the full-time Polytechnic Faculty and became University Professor Emeritus. He is now a part-time Professor of Aerospace and Mechanical Engineering and Professor of Electrical and Computer Engineering at Boston University, Boston, MA. He is the author or coauthor of more than 300 papers and several books, including *Radiation and Scattering of Waves* (Englewood Cliffs, NJ: Prentice-Hall, 1973; Piscataway, NJ: IEEE Press, 1994). He is an Associate Editor of several professional journals and an editor of the *Wave Phenomena Series* (New York: Springer-Verlag). His research interests encompass wave propagation and diffraction in complex environments and in various disciplines, high-frequency asymptotic and short-pulse techniques, and phase-space methods with an emphasis on wave-oriented data processing and imaging.

Dr. Felsen is a member of Sigma Xi and a Fellow of the Optical Society of America and the Acoustical Society of America. He has held named Visiting Professorships and Fellowships at universities in the United States and abroad, including the Guggenheim in 1973 and the Humboldt Foundation Senior Scientist Award in 1981. In 1974, he was an IEEE Antennas and Propagation Society (APS) Distinguished Lecturer. He received the Balthasar van der Pol Gold Medal from the International Union of Radio Science (URSI) in 1975, an honorary doctorate from the Technical University of Denmark in 1979, the IEEE Heinrich Hertz Gold Medal for 1991, the APS Distinguished Achievement Award for 1998, the IEEE Third Millennium Medal in 2000 (nomination by APS), three Distinguished Faculty Alumnus Awards from Polytechnic University, and an IEEE Centennial Medal in 1984. He also has received Best Paper awards for several papers in which he was an author or coauthor. In 1977, he was elected to the National Academy of Engineering. He served on the APS Administrative Committee from 1963 to 1966 and as Vice Chairman and Chairman for both the United States (1966–1973) and the International (1978–1984) URSI Commission B.

David A. Castañon (S'68–M'79–SM'98) received the B.S. degree in electrical engineering from Tulane University, New Orleans, LA, in 1971 and the Ph.D. degree in applied mathematics from the Massachusetts Institute of Technology (MIT), Cambridge, in 1976.

From 1976 to 1981, he was a Research Associate with the Laboratory for Information and Decision Systems, MIT. From 1982 to 1990, he was Senior and Chief Research Scientist at Alphatech, Inc., Burlington, MA. Since 1990, he has been a Professor in the Department of Electrical and Computer Engineering, Boston University, Boston, MA. His research interests include stochastic control and estimation, optimization, and image processing.

Dr. Castañon served as a member of the Board of Governors of the IEEE Control Systems Society. He is also a member of AMS, SIAM, and INFORMS.